Photonic arbitrary waveform generator based on Taylor synthesis method

Liao, Shasha; Ding, Yunhong; Dong, Jianji; Yan, Siqi; Wang, Xu; Zhang, Xinliang

Published in:
Optics Express

Link to article, DOI:
10.1364/OE.24.024390

Publication date:
2016

Document Version
Publisher's PDF, also known as Version of record

Research Article | Vol. 24, No. 21 | 17 Oct 2016 | OPTICS EXPRESS 24390

Optics EXPRESS

Photonic arbitrary waveform generator based on Taylor synthesis method

SHASHA LIAO,[1] YUNHONG DING,[2] JIANJI DONG,[1,*] SIQI YAN,[1,2] XU WANG,[1] AND XINLIANG ZHANG[1]

[1]*Wuhan National Laboratory for Optoelectronics, Huazhong University of Science and Technology, Wuhan 430074, China*

[2]*Department of Photonics Engineering, Technical University of Denmark, 2800 Kgs. Lyngby, Denmark*

[*]*jjdong@mail.hust.edu.cn*

Abstract: Arbitrary waveform generation has been widely used in optical communication, radar system and many other applications. We propose and experimentally demonstrate a silicon-on-insulator (SOI) on chip optical arbitrary waveform generator, which is based on Taylor synthesis method. In our scheme, a Gaussian pulse is launched to some cascaded microrings to obtain first-, second- and third-order differentiations. By controlling amplitude and phase of the initial pulse and successive differentiations, we can realize an arbitrary waveform generator according to Taylor expansion. We obtain several typical waveforms such as square waveform, triangular waveform, flat-top waveform, sawtooth waveform, Gaussian waveform and so on. Unlike other schemes based on Fourier synthesis or frequency-to-time mapping, our scheme is based on Taylor synthesis method. Our scheme does not require any spectral disperser or large dispersion, which are difficult to fabricate on chip. Our scheme is compact and capable for integration with electronics.

OCIS codes: (320.5540) Pulse shaping; (070.1170) Analog optical signal processing.

References and links

1. X. Fang, D.-N. Wang, and S. Li, "Fiber Bragg grating for spectral phase optical code-division multiple-access encoding and decoding," J. Opt. Soc. Am. B **20**(8), 1603–1610 (2003).
2. A. M. Weiner, "Ultrafast optical pulse shaping: A tutorial review," Opt. Commun. **284**(15), 3669–3692 (2011).
3. A. Monsterleet, S. Tonda-Goldstein, D. Dolfi, J. Huignard, P. Sapé, and J. Chazelas, "Optically generated arbitrary waveforms for radar applications," Electron. Lett. **41**(6), 332–334 (2005).
4. J.-J. Dong, B.-W. Luo, Y. Zhang, L. Lei, D.-X. Huang, and X.-L. Zhang, "All-optical temporal differentiator using a high resolution optical arbitrary waveform shaper," Chin. Phys. Lett. **29**(1), 014203 (2012).
5. A.-L. Zheng, J.-J. Dong, L. Lei, T. Yang, and X.-L. Zhang, "Diversity of photonic differentiators based on flexible demodulation of phase signals," Chin. Phys. B **23**(3), 033201 (2014).
6. F.-M. Kuo, J.-W. Shi, H.-C. Chiang, H.-P. Chuang, H.-K. Chiou, C.-L. Pan, N.-W. Chen, H.-J. Tsai, and C.-B. Huang, "Spectral power enhancement in a 100 GHz photonic millimeter-wave generator enabled by spectral line-by-line pulse shaping," IEEE Photonics J. **2**(5), 719–727 (2010).
7. Z. Jiang, D. E. Leaird, and A. M. Weiner, "Line-by-line pulse shaping control for optical arbitrary waveform generation," Opt. Express **13**(25), 10431–10439 (2005).
8. B. Bortnik, I. Y. Poberezhskiy, J. Chou, B. Jalali, and H. R. Fetterman, "Predistortion technique for RF-photonic generation of high-power ultrawideband arbitrary waveforms," J. Lightwave Technol. **24**(7), 2752–2759 (2006).
9. F. M. Soares, N. K. Fontaine, R. P. Scott, J. Baek, X. Zhou, T. Su, S. Cheung, Y. Wang, C. Junesand, S. Lourdudoss, K. Y. Liou, R. A. Hamm, W. Wang, B. Patel, L. A. Gruezke, W. T. Tsang, J. P. Heritage, and S. J. B. Yoo, "Monolithic InP 100-Channel 10-GHz Device for Optical Arbitrary Waveform Generation," IEEE Photonics J. **3**(6), 975–985 (2011).
10. N. K. Fontaine, R. P. Scott, J. Cao, A. Karalar, W. Jiang, K. Okamoto, J. P. Heritage, B. H. Kolner, and S. J. Yoo, "32 Phase X 32 amplitude optical arbitrary waveform generation," Opt. Lett. **32**(7), 865–867 (2007).
11. R. P. Scott, N. K. Fontaine, C. Yang, D. J. Geisler, K. Okamoto, J. P. Heritage, and S. J. Yoo, "Rapid updating of optical arbitrary waveforms via time-domain multiplexing," Opt. Lett. **33**(10), 1068–1070 (2008).
12. Y. Okawachi, K. Saha, J. S. Levy, Y. H. Wen, M. Lipson, and A. L. Gaeta, "Octave-spanning frequency comb generation in a silicon nitride chip," Opt. Lett. **36**(17), 3398–3400 (2011).
13. F. Ferdous, H. Miao, D. E. Leaird, K. Srinivasan, J. Wang, L. Chen, L. T. Varghese, and A. M. Weiner, "Spectral line-by-line pulse shaping of on-chip microresonator frequency combs," Nat. Photonics **5**(12), 770–776 (2011).

#272745 http://dx.doi.org/10.1364/OE.24.024390
Journal © 2016 Received 1 Aug 2016; revised 28 Sep 2016; accepted 7 Oct 2016; published 12 Oct 2016

Optics EXPRESS

14. H. Shen, L. Fan, L. T. Varghese, D. E. Leaird, A. M. Weiner, and M. Qi, "On-Chip Radio Frequency Arbitrary Waveform Generation," in *Conference on Lasers and Electro-Optics/ Quantum Electronics and Laser Sceince Conference,* (Optical Society of America, 2010), paper CMS2.
15. M. H. Khan, H. Shen, Y. Xuan, L. Zhao, S. Xiao, D. E. Leaird, A. M. Weiner, and M. Qi, "Ultrabroad-bandwidth arbitrary radiofrequency waveform generation with a silicon photonic chip-based spectral shaper," Nat. Photonics **4**(2), 117–122 (2010).
16. R. Slavík, Y. Park, N. Ayotte, S. Doucet, T.-J. Ahn, S. LaRochelle, and J. Azaña, "Photonic temporal integrator for all-optical computing," Opt. Express **16**(22), 18202–18214 (2008).
17. F. Zhang, J. Wu, Y. Li, and J. Lin, "Flat optical frequency comb generation and its application for optical waveform generation," Opt. Commun. **290**, 37–42 (2013).
18. A. Zhang and C. Li, "Analysis of dynamic optical arbitrary waveform generation based on three FBG arrays," Opt. Laser Technol. **52**, 81–86 (2013).
19. H.-Y. Jiang, L.-S. Yan, Y.-F. Sun, J. Ye, W. Pan, B. Luo, and X.-H. Zou, "Photonic arbitrary waveform generation based on crossed frequency to time mapping," Opt. Express **21**(5), 6488–6496 (2013).
20. A. Zhang and C. Li, "Dynamic optical arbitrary waveform generation with amplitude controlled by interference of two FBG arrays," Opt. Express **20**(21), 23074–23081 (2012).
21. M. Shen and R. A. Minasian, "Toward a high-speed arbitrary waveform generation by a novel photonic processing structure," IEEE Photonics Technol. Lett. **16**(4), 1155–1157 (2004).
22. R. A. Soref, "Silicon-based optoelectronics," Proc. IEEE **81**(12), 1687–1706 (1993).
23. N. N. Feng, P. Dong, D. Feng, W. Qian, H. Liang, D. C. Lee, J. B. Luff, A. Agarwal, T. Banwell, R. Menendez, P. Toliver, T. K. Woodward, and M. Asghari, "Thermally-efficient reconfigurable narrowband RF-photonic filter," Opt. Express **18**(24), 24648–24653 (2010).
24. J. Dong, A. Zheng, D. Gao, S. Liao, L. Lei, D. Huang, and X. Zhang, "High-order photonic differentiator employing on-chip cascaded microring resonators," Opt. Lett. **38**(5), 628–630 (2013).
25. M. H. Asghari and J. Azaña, "Proposal and analysis of a reconfigurable pulse shaping technique based on multi-arm optical differentiators," Opt. Commun. **281**(18), 4581–4588 (2008).
26. Y. Ding, H. Ou, and C. Peucheret, "Ultrahigh-efficiency apodized grating coupler using fully etched photonic crystals," Opt. Lett. **38**(15), 2732–2734 (2013).
27. Y. Ding, C. Peucheret, H. Ou, and K. Yvind, "Fully etched apodized grating coupler on the SOI platform with -0.58 dB coupling efficiency," Opt. Lett. **39**(18), 5348–5350 (2014).

1. Introduction

Optical arbitrary waveform generation (OAWG) attracts many attentions in recent years because it plays a critical role in many applications, such as generating optical ultra-wide band (UWB) signal [1,2], optical pulse radar [3], all optical temporal differentiator [4,5], and test of optical communication system. Many OAWG schemes have been proposed and they can be classified into several different methods according to the principle. The widely adopted ones are based on Fourier synthesis and frequency-to-time mapping. The schemes based on Fourier synthesis method usually consist of a source of optical frequency comb, spectral dispersers with high resolution and complex amplitude and phase modulation arrays. These schemes have very good performance and have been realized by different materials, such as mature fiber grating techniques [2,6–8], indium phosphide (InP) platform [9], silica on silicon [10,11], silicon nitride [12,13] and silicon platform [14–16]. However, high resolution integrated spectral disperser is still a big challenge for the chip fabrication resulting in the difficulty to manipulate the comb lines one by one when the comb spacing is very small. And the phase of comb lines is very sensitive to environmental fluctuation, making phase control very difficult and requiring coherent detection. The schemes based on frequency-to-time mapping usually consist of short pulse source, spectral shaper and dispersion medium which is used to realize the mapping. The source can be coherent light source [17,18] or incoherent light source [19]. And the spectral shaper can be obtained by using mature fiber grating techniques [20,21] or photonic integrated circuits. However, the dispersion medium is single mode fiber (SMF) or dispersion compensation fiber (DCF) in most of the schemes. To implement large dispersion on chip is still a big challenge.

In the paper, we propose and demonstrate a silicon on insulator (SOI) on chip optical arbitrary waveform generator based on Taylor synthesis method. Unlike other schemes based on Fourier synthesis method, we control the amplitude and phase of the differential waveform (Taylor series in time domain) of each tap instead of optical frequency comb lines. By thermally adjusting the amplitudes and phases of initial pulse, first-, second- and third-order

Optics EXPRESS

differential waveforms generated by cascaded microrings, we obtain several typical waveforms such as triangular waveform, sawtooth waveform, square waveform, flat-top waveform and Gaussian waveform, and so forth. Our scheme is compact, small power consumption and capable for integration with electronics [22,23]. Comparing with other schemes, our scheme has no requirements of high frequency resolution disperser, coherent detection and large dispersion.

2. Principle

In previous works, arbitrary waveforms were mostly obtained by using Fourier expansion method [2,6–17]. However, an arbitrary waveform can also be expanded by Taylor series [24] with

$$f(t)=f(0)+\frac{f'(0)}{1!}t+\frac{f''(0)}{2!}t^2+\frac{f'''(0)}{3!}t^3+\cdots+\frac{f^{(n)}(0)}{n!}t^n+R_n(t) \qquad (1)$$

where $f^{(n)}(t)$ is n-th derivative of $f(t)$, $R_n(t)$ is the remainder of Taylor formula. Because $R_n(t)$ is infinitesimal of higher order than t^n, we can ignore it. n-th derivative $g^{(n)}(t)$ of Gaussian pulse $g(t)$ can be expressed as

$$g^{(n)}(t)=\sum_{i=0}^{n}A_i t^i g(t) \qquad (2)$$

where A_i is a constant coefficient which can be calculated from the differentiation. When we combine original pulse and different order derivatives, we can get an equation as below

$$\frac{B_0 g(t)+B_1 g'(t)+B_2 g''(t)+B_3 g'''(t)+\cdots+B_n g^{(n)}(t)}{g(t)}=C_0+C_1 t+C_2 t^2+C_3 t^3+\cdots+C_n t^n \qquad (3)$$

The right part of the Eq. (3) is in the same form with Eq. (1). So we can obtain arbitrary waveforms by combining a Gaussian pulse and its different order derivatives with different weighting factors. In fact, other pulses more than Gaussian pulse can be the input pulse in Taylor synthesis method [25].

Figure 1 compares the schematic diagrams of arbitrary waveform generation by Fourier synthesis method and Taylor synthesis method. The upper part of Fig. 1 is the arbitrary waveform generation by Fourier synthesis method. This method combines a series of sinusoidal waves with different harmonic frequencies. The bottom part is based on Taylor synthesis method. A Gaussian pulse and its different order derivatives are combined with different weights to generate arbitrary waveforms. The schematic diagram of our on-chip pulse shaper is also shown in Fig. 2. The pattern structure is monolithically integrated on an SOI wafer, and it has the advantages of easy fabrication and compact footprint. The input Gaussian signal is divided into four taps by cascaded multimode interferometer (MMI) couplers, and then propagates through several microring resonators (MRRs), which are used to generate differential waveforms of the Gaussian pulse. An N-order differential can be considered as the input pulse multiplied by a filter with the transfer function of $(j(\omega-\omega_c))^N$, where ω_c is the optical carrier frequency. And the transfer function of an MRR just meets this requirement under critical coupling condition [24], so a single MRR can be a first-order differentiator and cascaded MRRs can realize a high-order differentiator. There is no MRR in the first tap, so the output of this tap is the initial Gaussian pulse. There is one MRR in the second tap resulting in first-order differentiation. Similarly, the output of the third and fourth taps is the second- and third-order differentiations of the input Gaussian pulse. There are an amplitude modulation unit (realized by a Mach-Zehnder interferometer (MZI) with one arm phase-modulated) and a phase modulation unit in each tap. All MRRs and phase modulation units are controlled by thermal electrodes. Assuming that the input Gaussian pulse and its derivatives are normalized and the

Optics EXPRESS

amplitudes and phases of them are set with α_0, α_1, α_2, α_3 and φ_0, φ_1, φ_2, φ_3, respectively, then the output of the pulse shaper can be expressed as

$$a(t)=\sum_{i=0}^{3}\alpha_i g^{(i)}(t)\exp(j\varphi_i) \tag{4}$$

$g^{(i)}(t)$ represents the i-th order derivative of Gaussian pulse with peak amplitude normalized to one. Our scheme has some advantages comparing with the schemes based on Fourier synthesis and frequency-to-time mapping. It is more compact because of using the MRRs as differentiators, and does not require a precise disperser for line by line shaping or an on-chip large dispersion.

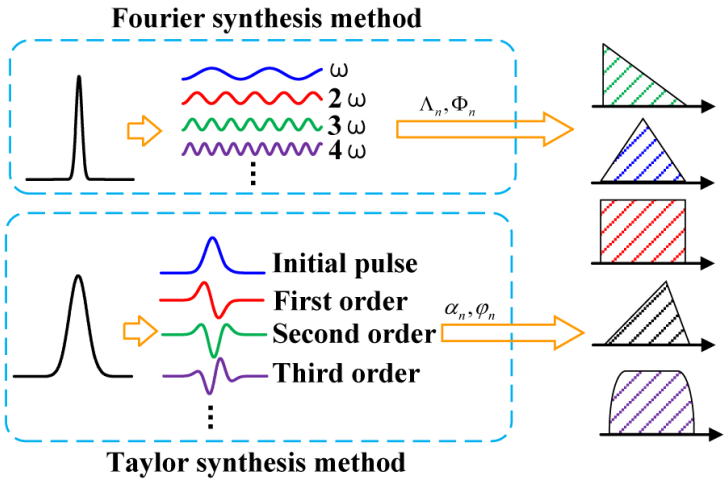

Fig. 1. Schematic diagrams of arbitrary waveform generations by Fourier synthesis method and Taylor synthesis method.

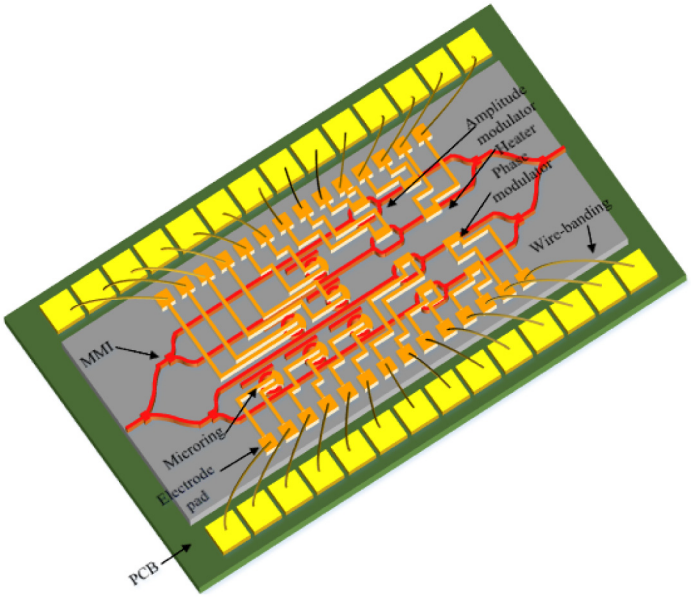

Fig. 2. Schematic diagram of the proposed on-chip pulse shaper.

Optics EXPRESS

First of all, the central frequency of input Gaussian pulse is aligned to the notch of the MRRs to obtain the differentiations. And by jointly tuning both amplitude and phase arrays of the input Gaussian pulse and its derivatives we can achieve several typical waveforms. The amplitude and phase array of target waveform can be calculated according to Taylor expansion. Figure 3(a) shows the input Gaussian pulse with a full width at half maximum (FWHM) of 61.8 ps. By setting the amplitude array and phase array to α = [1, 0.27, 0.32, 0.09] and φ = [0, 0.5π, 0, 0.5π], respectively, we can obtain a square waveform which is shown in Fig. 3(b). The FWHM of the simulated square waveform is 113.1 ps. Figure 3(c) shows an isosceles triangular waveform generated by this pulse shaper. In this case, the amplitude array and phase array are α = [0.25, 0.15, 1, 0.51] and φ = [0, 0.6π, 0, 1.47π], respectively. The FWHM of the simulated isosceles triangular waveform is 121.2 ps. Then we simulate a super-Gaussian waveform by setting the amplitude and phase array to α = [1, 0.03, 0.31, 0.06] and φ = [0, π, 0, 1.35π], respectively. In order to achieve two opposite sawtooth waveforms, we can just set the amplitude and phase arrays to α = [0.41, 0.39, 1, 0.42], φ = [1.1π, 0.99π, 1.38π, 0] and α = [0.46, 0.79, 1, 0.53], φ = [0, 1.03π, 0.2π, 1.25π], respectively. The corresponding simulated waveforms are shown in Figs. 3(d), 3(e) and 3(f). The FWHMs of the simulated super-Gaussian pulse and the sawtooth waveforms are 105.1 ps, 85.9 ps and 73.6 ps. In order to demonstrate that our scheme can generate more general waveforms, we simulated two opposite oblique triangular waveforms and a Gaussian waveform. The amplitude and phase arrays of the two opposite oblique triangular waveforms are α = [1, 0.88, 0.88, 0.32], φ = [0, 1.95π, 1.7π, 0] and α = [1, 0.06, 0.03, 0.09], φ = [1.9π, π, 0, 1.5π], respectively, and the FWHMs are 68.1 ps and 94.4 ps. The corresponding simulated waveforms are shown in Figs. 3(g) and 3(h). And the Gaussian waveform with an FWHM of 85.9 ps is shown in Fig. 3(i). And the amplitude and phase arrays are α = [1, 0, 0.21, 0.02] and φ = [0, 0, 0, 1.3π], respectively. Finally, we set the amplitude and phase arrays to α = [0, 1, 0, 0] and φ = [0, 0, 0, 0], respectively, and we can obtain the first-order differentiation of the input pulse which is shown in Fig. 3(j). The amplitude and phase arrays of all simulated waveforms are shown in Table 1 for concision. The ideal waveforms of the corresponding waveforms are also shown in the Figs. 3(b)-3(j) (red dash line) for comparison. As shown in Figs. 3(c)-3(j), the simulated waveforms are in good agreements with the ideal ones. The simulated square waveform which is shown in Fig. 3(b) has larger distortion with the ideal one than other simulations, because the square waveform has very sharp edges which need higher-order differentiation components.

Optics EXPRESS

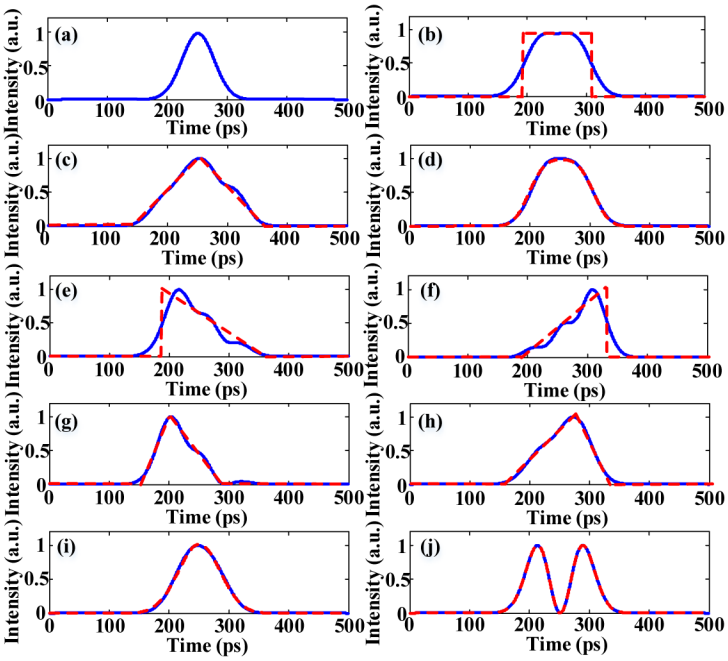

Fig. 3. Simulated waveforms (blue solid line) of the pulse shaper and the ideal ones (red dash line) of (a) input Gaussian pulse, (b) square waveform (the amplitude array and phase array are [1, 0.27, 0.32, 0.09] and [0, 0.5π, 0, 0.5π], respectively), (c) isosceles triangular waveform (the amplitude array and phase array are [0.25, 0.15, 1, 0.51] and [0, 0.6π, 0, 1.47π], respectively), (d) super-Gaussian waveform (the amplitude array and phase array are [1, 0.03, 0.31, 0.06], and [0, π, 0, 1.35π], respectively), (e) and (f) sawtooth waveforms (the amplitude array and phase array are [0.41, 0.39, 1, 0.42], [1.1π, 0.99π, 1.38π, 0] and [0.46, 0.79, 1, 0.53], [0, 1.03π, 0.2π, 1.25π], respectively), (g) and (h) oblique triangular waveforms (the amplitude array and phase array are [1, 0.88, 0.88, 0.32], [0, 1.95π, 1.7π, 0] and [1, 0.06, 0.03, 0.09], [1.9π, π, 0, 1.5π], respectively), (i) Gaussian waveform (the amplitude array and phase array are [1, 0, 0.21, 0.02] and [0, 0, 0, 1.3π], respectively) and (j) first-order differentiation (the amplitude array and phase array are [0, 1, 0, 0] and [0, 0, 0, 0], respectively).

Table 1. Amplitude and phase arrays of the simulated waveforms

Waveform type	Amplitude array				Phase array			
	α_0	α_1	α_2	α_3	φ_0	φ_1	φ_2	φ_3
Square	1	0.27	0.32	0.09	0	0.5π	0	0.5π
Isosceles triangular	0.25	0.15	1	0.51	0	0.6π	0	1.47π
Super-Gaussian	1	0.03	0.31	0.06	0	π	0	1.35π
Sawtooth 1	0.41	0.39	1	0.42	1.1π	0.99π	1.38π	0
Sawtooth 2	0.46	0.79	1	0.53	0	1.03π	0.2π	1.25π
Oblique triangular 1	1	0.88	0.88	0.32	0	1.95π	1.7π	0
Oblique triangular 2	1	0.66	0.03	0.09	1.9π	π	0	1.5π
Gaussian waveform	1	0	0.21	0.02	0	0	0	1.3π
First-order differentiation	0	1	0	0	0	0	0	0

Optics EXPRESS

3. Experimental verification

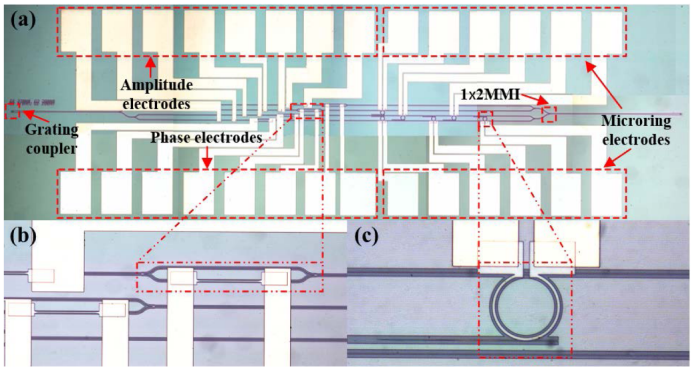

Fig. 4. Metallurgical microscopy image of the on-chip pulse shaper, (a) whole graph, details of (b) MZI and (c) MRR.

The microscopic image of our pulse shaper is shown in Fig. 4(a). The pulse shaper is fabricated on an SOI wafer with 250 nm thick top silicon layer and 3 μm thick buried oxide (BOX). The height of the waveguide is 250 nm and the width is 450 nm. The six MRRs are all the same size with a radius of 20 μm. In order to get larger extinction ratio, the MRRs are all add-drop ones, and the two gaps of the MRR are 230 nm and 240 nm, respectively. The size of our pulse shaper is about 4 mm^2. We use fully etched apodized grating couplers [26] for the coupling between fiber and chip. There are five steps in the fabrication. The first step is to simultaneous fabricate the grating couplers and silicon waveguides. Here we use a single step of E-beam lithography and inductively coupled plasma reactive ion etching (ICP-RIE). The second step is to deposit a 700 nm thick silica on the sample. Depositing another 700 nm layer of boro-phospho-silicate-glass (BPSG) is the third step. It is annealed in nitrogen condition and for planarizing the surface. After that, the top glass layer is thinned to 1μm by buffered hydrofluoric acid (BHF) etching. The last step is to fabricate the heaters. The heater patterns (100 nm Ti) are formed by E-beam lithography followed by metal deposition and lift-off. The fiber-to-fiber loss of our pulse shaper is about 22 dB when there is no voltage applied to the electrodes. And the loss of the waveguide and grating are 2 dB/cm and 3 dB/port, respectively. And the loss of the MMI and MMR are both less than 0.2 dB. And the loss of the modulators is less than 0.4 dB. All four taps are fabricated with metal thermal conductors to tune the amplitude and phase respectively. And the MRRs are also fabricated with metal thermal conductors to tune the resonant wavelengths. The insertion loss can be effectively reduced by introducing an aluminum mirror by flip-bonding process [27]. Figures 4(b) and 4(c) show the details of MZI and MRR.

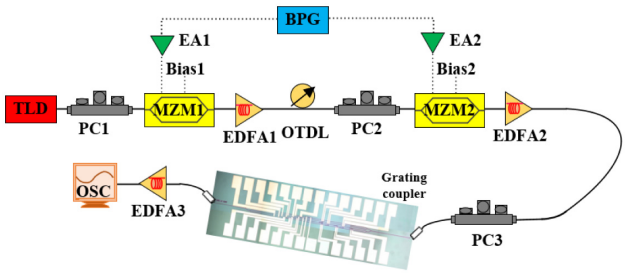

Fig. 5. Experimental setup of the arbitrary waveform generation with employing the on-chip pulse shaper. (TLD: tunable laser diode, PC: polarization controller, MZM: Mach-Zehnder modulator, BPG: bit pattern generator, EA: electronic amplifier, OTDL: optical time delay, EDFA: erbium-doped fiber amplifier, OSC: oscilloscope).

Optics EXPRESS

The experimental setup for the arbitrary waveform generation is shown in Fig. 5. A continuous wave (CW) light is emitted from the tunable laser diode (TLD). And the light is modulated by two cascaded Mach–Zehnder modulators (MZMs), which are driven by a bit pattern generator (BPG) at a bit rate of 10 Gbit/s with code "1000". So the repetition period of the input Gaussian pulse is 400 ps. The wavelength of the CW light is aligned to the resonant wavelength of the MRRs. And the slight drifts of the resonant wavelengths of the MRRs are calibrated by the thermal electrodes. We use two polarization controllers (PCs) before the MZMs because of the polarization sensitivity. Two erbium doped fiber amplifiers (EDFAs) connected at the output of the MZMs are used to amplify the optical signal. An optical tunable delay line (OTDL) is used to synchronize the data signal applied on the MZMs. Two vertical grating couplers are used to couple the light from fiber to silicon waveguide and the output signal from waveguide to fiber. And another PC is also placed before the input grating coupler. To simplify the experiment operations, we use wire-bonding technique. Firstly, we bond the electrode pads on chip with the electrodes on a printed circuit board (PCB) and then external wires are pasted on the electrodes by conductive adhesive. We use independent power supplies to apply variable voltages to the heaters by the external wire. And a high speed oscilloscope (OSC, Agilent 86100C) is used to measure the output temporal waveform.

Figure 6(a) shows the measured input Gaussian pulse with a FWHM of 60 ps. The measured square waveform is shown in Fig. 6(b). The FWHM of the measured waveform is 108.9 ps. In order to achieve this waveform, we should adjust all the voltages applied on the amplitude electrodes and phase electrodes to match with the simulated condition. In experiment, the differentiations have some loss when generated by MRRs, so the coefficient of the amplitude array is not the same with simulated one. The coefficients of the amplitude and phase arrays are shown in Table 2. We also achieve isosceles triangular waveform, which is shown in Fig. 6(c) as the blue solid line, and the FWHM is 125.2 ps. A super-Gaussian waveform with the FWHM of 107.4 ps is shown in Fig. 6(d). And two opposite sawtooth waveforms are shown in Figs. 6(e) and 6(f) with the FWHM of 84.4 ps and 70.4 ps, respectively. Figures 6(g) and 6(h) are two opposite oblique triangular waveforms with the FWHMs of 64.5 ps and 97.4 ps, respectively. And the Gaussian waveform is shown in Fig. 6(i), the FWHM of the measured waveform is 83.4 ps. And at last the measured first-order differentiation is shown in Fig. 6(j), the FWHMs is 131.1 ps. The ideal ones are also shown as the red dash line for comparison. In order to analyze the distortions between the measured waveforms and the ideal ones, we use a total average error to represent the distortions. The error can be expressed as:

$$Error = \frac{1}{T}\int_{T} \left| P_m(t) - P_i(t) \right| \cdot dt \tag{5}$$

where $P_m(t)$ and $P_i(t)$ are the power of measured waveforms and ideal waveforms, respectively, and T is the time period which is 400 ps in our scheme. The average errors of the measured waveforms are shown in Table 3. The maximum average error is less than 10%, which means that the measured waveforms are consistent to the ideal ones, so our scheme has a good performance on waveform generation.

Optics EXPRESS

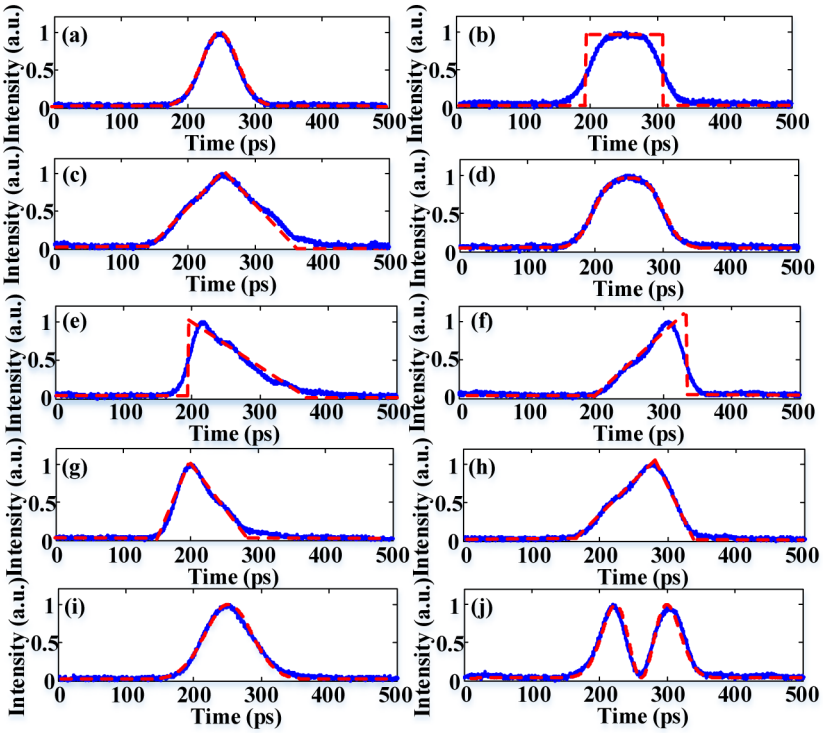

Fig. 6. Measured waveforms (blue solid line) of the pulse shaper and ideal ones (red dash line) of (a) input Gaussian pulse, (b) square waveform, (c) isosceles triangular waveform, (d) super-Gaussian waveform, (e) and (f) sawtooth waveform, (g) and (h) oblique triangular waveform, (i) Gaussian waveform and (j) first-order differentiation.

Table 2. Amplitude and phase arrays of the measured waveforms

Waveform type	Amplitude array				Phase array			
	α_0	α_1	α_2	α_3	φ_0	φ_1	φ_2	φ_3
Square	1	0.57	0.59	0.27	0	0.5π	0	0.5π
Isosceles triangular	0.14	0.17	1	0.84	0	0.6π	0	1.47π
Super-Gaussian	1	0.06	0.57	0.18	0	π	0	1.35π
Sawtooth 1	0.22	0.45	1	0.69	1.1π	0.99π	1.38π	0
Sawtooth 2	0.25	0.91	1	0.87	0	1.03π	0.2π	1.25π
Oblique triangular 1	0.53	1	0.87	0.52	0	1.95π	1.7π	0
Oblique triangular 2	0.71	1	0.04	0.2	1.9π	π	0	1.5π
Gaussian waveform	1	0	0.39	0.06	0	0	0	1.3π
First-order differentiation	0	1	0	0	0	0	0	0

Table 3. Average errors of the measured waveforms

Waveform type	Error	Waveform type	Error	Waveform type	Error
Square	9.9%	Isosceles triangular	3.3%	Super-Gaussian	3.4%
Sawtooth1	6.5%	Sawtooth2	6.8%	Oblique triangular 1	4.0%
Oblique triangular 2	3.4%	Gaussian	3.3%	First-order differentiation	6.5%

The average errors of the generated waveforms mostly result from the limitation of number of the taps. And if we increase taps in our pulse shaper, the average errors can be reduced. We simulate the average errors of the triangular waveform and square waveform using different taps, and the results are shown in Fig. 7. The red circle dot is the calculate errors of the

Optics EXPRESS

triangular waveform, and the blue square is that of the square waveform. The orange and black lines are the numerical fittings of the measured dots. The error of the triangular waveform decreases from 3.2% to 1.4% when the number of taps increasing from 4 to 11. And the error of square waveform decreases from 7.5% to 5%. So we can obtain more precise waveform with larger number of taps. And in our scheme, there should be n-1 MMRs on the n-th tap, the whole system will be quite huge when n is large. But we can use an asymmetric MMI after the (n-1)-th differentiation to split the signal to two taps: one tap for amplitude and phase modulation, and the other tap is launched into an MMR for the n-th differentiation. The MMI can be a power splitter and balancer simultaneously. In this way, the chip size of the pulse shaper will be greatly reduced.

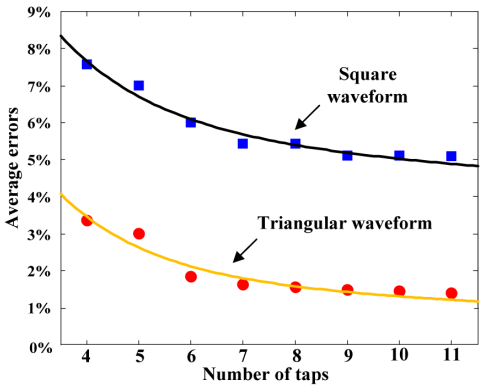

Fig. 7. Average errors of the triangular waveform and square waveform with different taps.

Complete controlling of the amplitude modulators and phase modulators is very important in our scheme. For simplification, we only test the amplitude modulators. We adjust the central wavelength of the input pulse to make it far from the resonant wavelength of the MRRs. And we jointly tune amplitude modulators on each tap to make the output power zero. Then we choose one of the amplitude modulator and vary the voltage from 0 V to 7 V. Figure 8(a) shows the output power varying with the voltage applied on to the electrode as the blue dots. The red solid line is a numerical fitting of the measured dot. Figure 8(b) shows four examples of different output power of the output pulse. It is obvious that the amplitude modulator in our scheme can be completely controlled. The power consumption varies when the pulse shaper is in different functions, and the maximum power consumption is about 350 mW. The bandwidth of the generated waveform is limited by the bandwidth of input Gaussian pulse and the operation bandwidth of the MRRs. In our scheme the operation bandwidth of the MRRs is about 10.5 GHz.

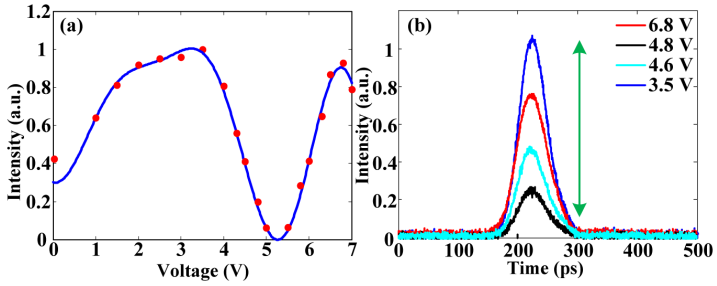

Fig. 8. (a) Output power varies with the voltage applied on to the electrode (measured power is shown as blue dot and numerical fitting is shown as red solid line), and (b) four examples of different output power of output pulse.

Optics EXPRESS

4. Conclusions

We have proposed and demonstrated a photonic arbitrary waveform generator based on a silicon integrated circuit. Unlike other widely adopted schemes using Fourier synthesis method, our scheme is based on Taylor synthesis method. Firstly, we use cascaded MRRs to generate first-, second- and third-order differentiations of the input Gaussian pulse. Then, we adjust the voltages to control the amplitudes and phases of the initial pulse, first-, second- and third-order differentiations. Finally, we combine these signals to implement several typical waveforms such as square waveform, isosceles triangular waveform, sawtooth waveform, oblique triangular waveform, Gaussian waveform and super-Gaussian waveform. And we also analyzed the distortions between the generated waveforms and ideal ones and verified the complete amplitude control of our pulse shaper. Our scheme is compact because of employing MRRs, and has advantages of small power consumption and capability for integration with electronics. Comparing with Fourier synthesis schemes and frequency to time mapping schemes, our scheme does not require high frequency resolution disperser, coherent detection or large dispersion reducing the complexity of fabrication.

Funding

New Century Excellent Talents in Ministry of Education of China (NCET-11-0168); National Excellent Doctoral Dissertation of China (201139); National Natural Science Foundation of China (NSFC) (61622502, 61475052).